SCIENCE CHINA
Life Sciences

•COVER ARTICLE•

December 2022 Vol.65 No.12: 2341–2353
https://doi.org/10.1007/s11427-022-2194-7

Causal gene identification and desirable trait recreation in goldfish

Peng Yu[1], Yang Wang[1,2], Zhi Li[1], Hui Jin[1,2], Liang-Liang Li[1,2], Xiao Han[1,2], Zhong-Wei Wang[1,2], Xiao-Li Yang[1,2], Xi-Yin Li[1,2], Xiao-Juan Zhang[1], Li Zhou[1,2*] & Jian-Fang Gui[1,2*]

[1]*State Key Laboratory of Freshwater Ecology and Biotechnology, Hubei Hongshan Laboratory, The Innovation Academy of Seed Design, Institute of Hydrobiology, Chinese Academy of Sciences, Wuhan 430072, China;*
[2]*University of Chinese Academy of Sciences, Beijing 100049, China*

Received July 7, 2022; accepted August 11, 2022; published online November 10, 2022

Goldfish (*Carassius auratus*) have long fascinated evolutionary biologists and geneticists because of their diverse morphological and color variations. Recent genome-wide association studies have provided a clue to uncover genomic basis underlying these phenotypic variations, but the causality between phenotypic and genotypic variations have not yet been confirmed. Here, we edited proposed candidate genes to recreate phenotypic traits and developed a rapid biotechnology approach which combines gene editing with high-efficiency breeding, artificial gynogenesis, and temperature-induced sex reversal to establish homozygous mutants within two generations (approximately eight months). We first verified that *low-density lipoprotein receptor-related protein 2B* (*lrp2aB*) is the causal gene for the dragon-eye variation and recreated the dragon-eye phenotype in side-view Pleated-skirt Lion-head goldfish. Subsequently, we demonstrated that the albino phenotype was determined by both homeologs of *oculocutaneous albinism type II* (*oca2*), which has subfunctionalized to differentially govern melanogenesis in the goldfish body surface and pupils. Overall, we determined two causal genes for dragon-eye and albino phenotypes, and created four stable homozygous strains and more appealing goldfish with desirable traits. The developed biotechnology approach facilitates precise genetic breeding, which will accelerate re-domestication and recreation of phenotypically desirable goldfish.

goldfish, precise molecular design breeding, re-domestication, gene editing, ornamental traits, dragon-eye, albino

Citation: Yu, P., Wang, Y., Li, Z., Jin, H., Li, L.L., Han, X., Wang, Z.W., Yang, X.L., Li, X.Y., Zhang, X.J., et al. (2022). Causal gene identification and desirable trait recreation in goldfish. Sci China Life Sci 65, 2341–2353. https://doi.org/10.1007/s11427-022-2194-7

INTRODUCTION

Goldfish were the first domesticated ornamental fish, with domestication dating back approximately 1800 years in China, and have been developed into more than 300 strains with diverse morphological and color variations (Chen, 1954; Gui et al., 2022; Omori and Kon, 2019; Ye and Qu, 2017). Because of their fascinating phenotypic traits and allotetraploid genome (Zhou and Gui, 2017), goldfish have become both a popular ornamental fish worldwide and a model organism in evolutionary genetics (Chen et al., 2020; Kon et al., 2020; Luo et al., 2020; Ota and Abe, 2016). Genome-wide association studies revealed six candidate genes that may be associated with several representative phenotypes, including twin-tail, long-tail, heart-shaped tail, dorsal fin loss, telescope-eye (dragon-eye), and albino phenotypes (Kon et al., 2020), and two different genomic regions were speculated to be associated with dorsal fin loss and transparent scales (Chen et al., 2020). However, the causal link between phenotypic variations and genetic loci has not yet been confirmed.

Currently, most goldfish strains are suitable for top viewing in pots, and many phenotypic variations, including Dragon-eye and Albino, have been retained in these strains. With the popularity of fish tanks and ever-changing aes-

*Corresponding authors (Li Zhou, email: zhouli@ihb.ac.cn; Jian-Fang Gui, email: jfgui@ihb.ac.cn)

thetics, goldfish enthusiasts favor specific variations for side viewing. However, only a few strains have been bred that are suitable for side viewing, such as Pleated-skirt Lion-head goldfish and Ranchu goldfish. Supported by continuous advances and innovations in genomic biotechnology, several novel breeding approaches, including key gene editing-based molecular breeding technology, have been applied in some aquaculture species and have the potential to expedite their genetic improvement, especially in fishes with a long sexual maturation cycle (Gui et al., 2022; Houston et al., 2020). Gene editing can remove undesirable traits by knockout of key genes or improve desirable traits by the introduction of favorable alleles from other strains/species or even by the creation of *de novo* alleles (Abdelrahman et al., 2017; Gratacap et al., 2019; Gui et al., 2022; Houston et al., 2020; Nie et al., 2022; Okoli et al., 2022; Sun and Zhu, 2019). Therefore, key gene editing-based molecular breeding that allows the precise transfer and fixation of a desired trait from top-view goldfish to side-view goldfish would enable to quick recreation of novel or tailored strains. Although gene editing is very difficult in tetraploid goldfish (Kon et al., 2020), in this study, we developed a new biotechnology approach to rapidly construct homozygous strains and applied it to recreate some preferred phenotypic traits in side-view strains. The current study improves our understanding of molecular mechanisms underlying the formation of diverse goldfish phenotypes and develops an efficient approach to rapidly recreate desirable traits in goldfish or other aquaculture fishes.

RESULTS

Identification of candidate gene for the dragon-eye phenotype

To identify and verify the genetic locus associated with the dragon-eye phenotype, we *de novo* created a novel homozygous Dragon-eye strain from common goldfish with normal eyes (Figure 1A) and demonstrated that dragon-eye is a recessive trait controlled by a major gene (Yu et al., 2021) (Figure S1 in Supporting Information). Whole-genome resequencing (WGR)-based bulked-segregant analysis (BSA) was performed on one F3 segregated population. After filtering (Figure S2A in Supporting Information), a total of 3,302,137 SNPs that were homozygous (the reference genotype) in the dragon-eyed paternal parent but heterozygous in the normal-eyed maternal parent were retained to identify the candidate mutation(s). For each SNP site, the SNP index (the ratio of non-reference reads to the total reads mapped to the variation site) in two DNA bulks of the F3 segregated population was calculated. Graphs were generated that depicted the relationship between the SNP index and SNP positions in the assembled reference genome (Figure 1B, Figure S2B in Supporting Information). The causative SNP should be homozygous in the dragon-eyed offspring, same as that in the reference genotype, and therefore have an SNP index = 0. However, it should be heterozygous in normal-eyed offspring, resulting in an SNP index = ~0.5. Therefore, the dragon-eye phenotype was mapped to six candidate genomic regions in four chromosomes; these regions ranged from 0.21 to 6.49 Mb and harbored 201 genes (Figure 1B, Figure S2B in Supporting Information).

Combining comparative transcriptomics and large-effect SNP analysis revealed four candidate genes in *C. auratus* chromosome 9B (*Ca* 9B): *low-density lipoprotein receptor-related protein 2B* (*lrp2aB*), *gap junction gamma-1B protein* (*gjc1B*), *striated muscle preferentially expressed protein kinase B* (*spegB*), and *protocadherin-8-like B* (*pcnsB*); these genes had SNPs in the start/stop codon and were differentially expressed between individuals with normal-eye and dragon-eye phenotypes (Fragments Per Kilobase of exon model per Million mapped fragments, FPKM > 1) (Figure 1C, Figure S2C in Supporting Information). Of these SNPs, only one in the 73rd exon of *lrp2aB* was determined to be present in the dragon-eyed population based on PCR and sequencing. Detailed sequence analysis showed that the codon of Gly^{4469} (GGA) mutated into a stop codon (TGA) in the Dragon-eye strain (Lrp2$^{G4469X/G4469X}$, where "X" is used to show a stop codon in a protein sequence) (Figure 1D, E), which resulted in a truncated protein that lacked the majority of its C-terminal cytoplasmic tail, including two NPXY motifs and one PDZ domain binding motif (Figure 1F). The same stop codon mutation was also identified in Butterfly Moor goldfish (Figure S3 in Supporting Information). Our previous study revealed that the amount of lipid droplets in eyelid connective tissue was increased in individuals with the dragon-eye phenotype compared with those with normal eyes (Yu et al., 2021); this indicated that lipid transport and storage play a role in the morphological and structural transformation that produces the dragon-eye phenotype.

Precise breeding biotechnology establishment and dragon-eye recreation

To confirm the role of *lrp2aB* in the morphological variation of dragon-eye, we first developed a rapid biotechnology technique to establish homozygous mutants in goldfish within two generations. This approach combines high-efficiency breeding, gene editing, artificial gynogenesis, and temperature-induced sex reversal (Figure 1G).

Generally, goldfish take one year for a generation, and sufficient nutrition is the key to goldfish's rapid sexual maturity and multiple spawning. In this study, goldfish were fed at least four times and up to seven times per day (Table S1 in Supporting Information), which exceeds the typical feeding regimen (twice a day). Animal baits, such as live nauplii,

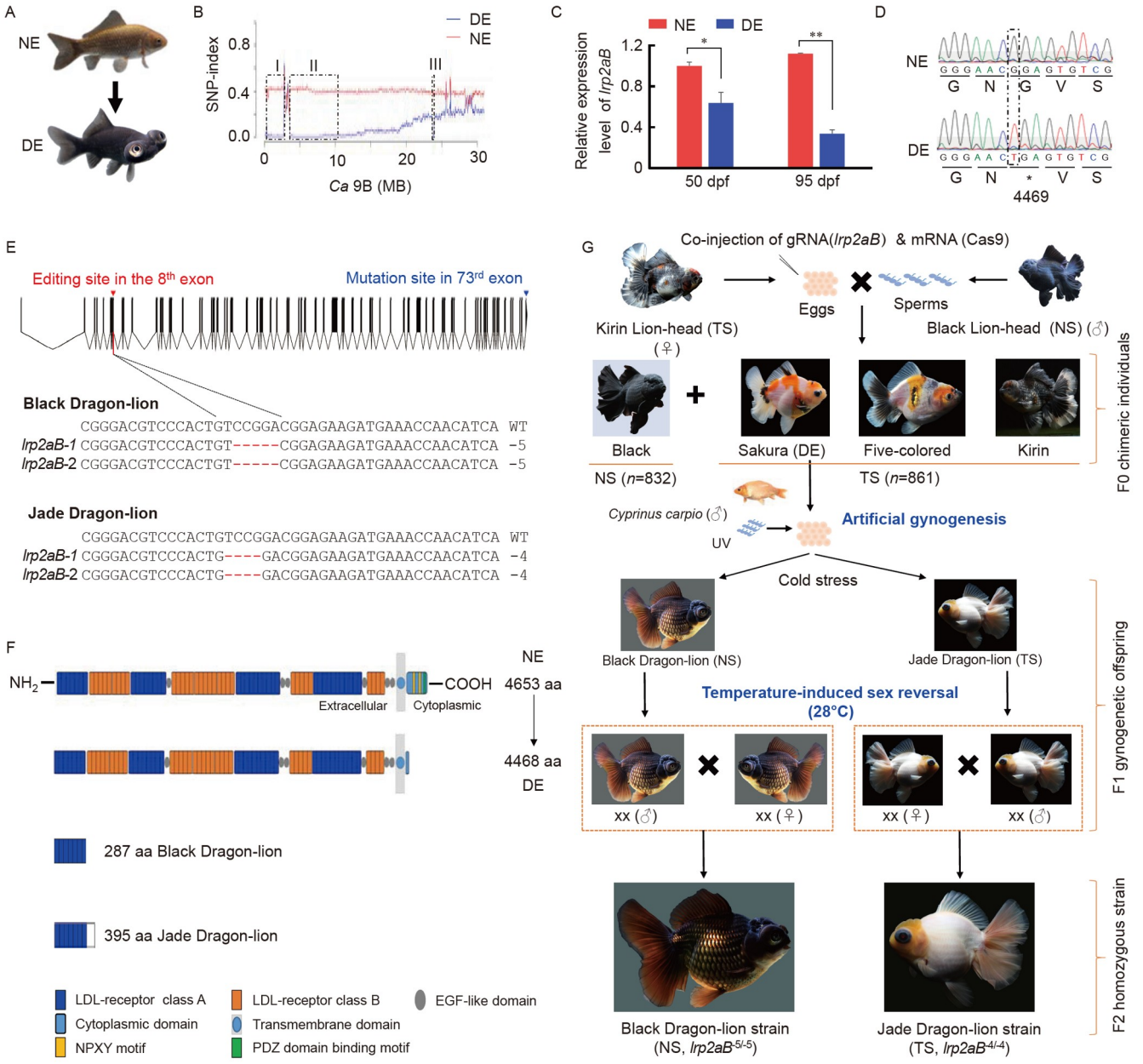

Figure 1 Identification of *lrp2aB* as a causal gene associated with the dragon-eye phenotype in goldfish. A, *de novo* created Dragon-eye (DE) *C. auratus* and WT with normal-eye (NE). B, SNP index plot of *C. auratus* chromosome 9B (*Ca* 9B) showing three genomic regions (I, II, and III) with SNP index = 0 in DE and SNP index = ~0.5 in NE. The red and blue lines represent the sliding window average values of the SNP index at 100-kb intervals with 10-kb increments for NE and DE, respectively. C, qPCR analyses of *lrp2aB* in NE and DE at 50 (before protruding) and 95 dpf (after protruding), *, $P<0.05$, **, $P<0.01$. *β-actin* was used to normalize data. The expression level of NE at 50 dpf was set as 1. Each bar represents the mean±SD ($n=3$). D, A missense mutation (G4469X) was identified in the *C. auratus* DE strain. A glycine codon (GGA) mutated into a stop codon (TAG) at amino acid position 4469. E, Mutated sequences of *lrp2aB* in two homozygous *lrp2aB*$^{-/-}$ strains. Exons and introns were depicted as rectangular boxes and thick lines. WT *lrp2aB* has 73 exons, the mutation site of *lrp2aB* was located in the 73rd exon, and the target site was chosen from the 8th exon. F, Schematic representation of truncated Lrp2aB proteins in the *C. auratus* DE strain and two homozygous *lrp2aB*$^{-/-}$ strains. G, Establishment of two homozygous *lrp2aB*$^{-/-}$ strains by CRISPR/Cas9, artificial meiotic gynogenesis, and temperature-induced sex reversal. Goldfish eggs fertilized by UV-irradiated *C. carpio* sperm were treated by cold shock (0–2°C) for 30 min at 6 min post-fertilization. The gynogenetic offspring were identified by morphological differences. NS, normal scale; TS, transparent scale.

water angleworm, or frozen chironomid larvae, are necessary for high-efficiency propagation. Moreover, the filtration system is needed to keep goldfish in good condition. Through these measures, goldfish can spawn at approximately 4 months post-fertilization and are able to spawn again every 4–7 days in all year around with approximately 40 times (Figure 2A). The improved raising conditions include a nutritious diet (overfed, 4–7 times per day) (Table S1 in Supporting Information), filtered water (pH 7–8, 24–28°C), adequate light (18 h light and 6 h dark), sufficient

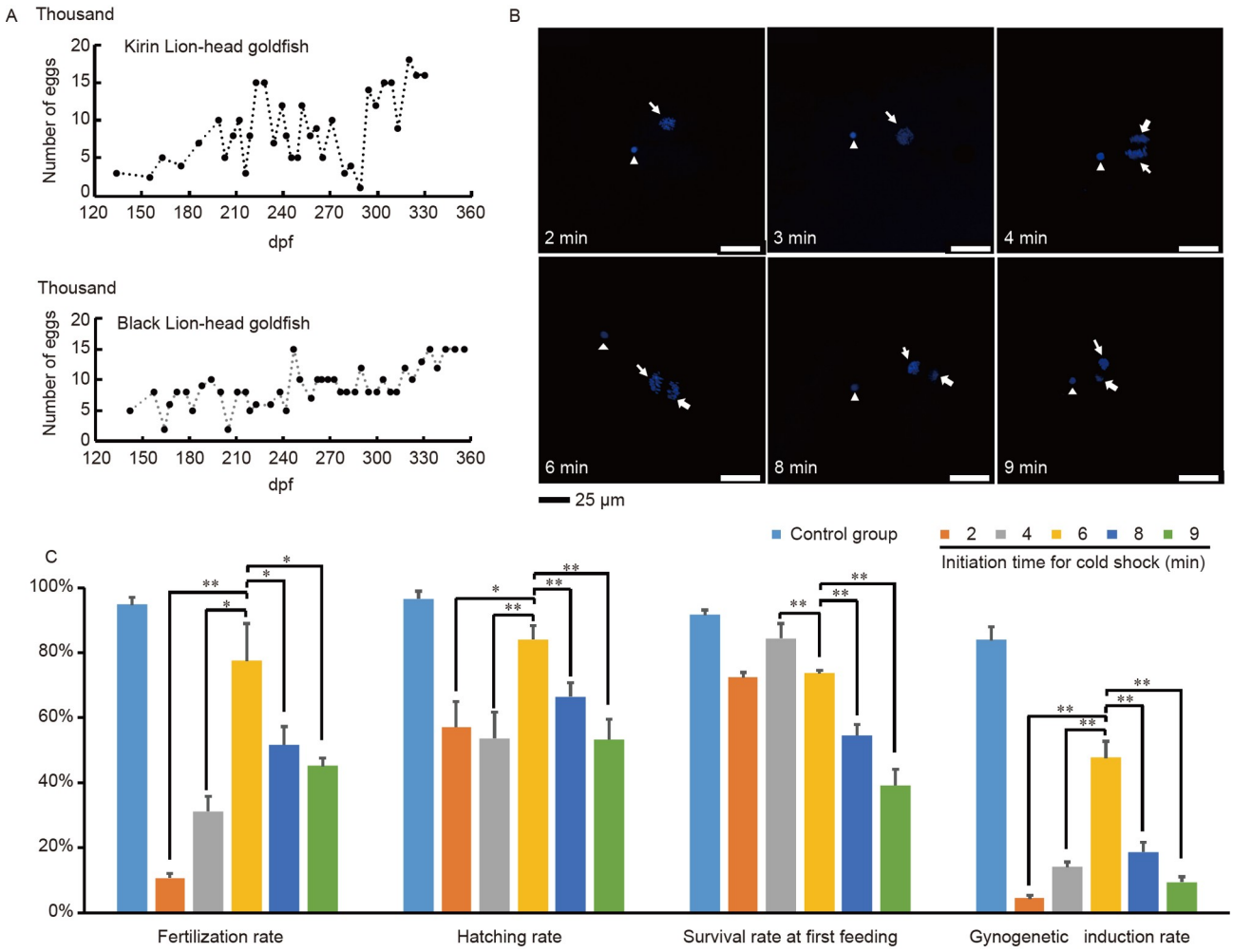

Figure 2 High-efficiency breeding and artificial gynogenesis in goldfish. A, Time of initial sexual maturity and number of eggs spawned each time in two goldfish females under improved raising conditions. The Kirin Pleated-skirt Lion-head goldfish female started to lay eggs at 134 dpf and spawned every 5.9±3.6 days year-round, for a total of 34 times, and a single clutch contained 8,800±4,700 eggs (top). The Black Pleated-skirt Lion-head goldfish spawned 42 times in 215 days and a single clutch contained 8,900±3,300 eggs (bottom). B, DAPI-stained nucleus behaviors at 2, 3, 4, 6, 8, and 9 min post-fertilization in the fertilized goldfish eggs. The eggs of Kirin Pleated-skirt Lion-head goldfish were fertilized by Black Lion-head goldfish sperm. Scale bars, 25 μm. The male pronucleus, female pronucleus, and second polar body were determined by the shape and size of nuclei and they are indicated with arrowheads, thin arrows, and thick arrows, respectively. C, Effects of cold shock initiation time on the fertilization rate, hatching rate, survival rate at first feeding, and gynogenesis induction rate. The duration time of cold shock treatment was 30 min. The gynogenesis induction rate (47.7%±5.1%) was the highest at 6 min post-fertilization. Each bar represents the mean±SD (n=3).

oxygen (7–9 mg L^{-1}), and low fish density (1 fish/30–50 L). Therefore, the high-efficiency breeding method allows goldfish to produce thousands of eggs (8,862±3,951 per time) all year round.

The high-efficiency breeding technique provides sufficient eggs to determine the optimal conditions for artificial gynogenesis, which is often used to purify homozygous alleles in fish (Zhou et al., 2018). The cold shock initiation time is critical to the induction rate of artificial gynogenesis and varies among different species (Zhou and Gui, 2017). Our previous study on Lanzhou catfish (*Silurus lanzhouensis*) suggested that the optimal initiation time is the period when the second polar body is completely separated from the female pronucleus but not starts to condense (Wang et al., 2021). Therefore, we observed the nuclear behaviors via DAPI staining in the fertilized goldfish eggs. As shown in Figure 2B, the second polar body and the female pronucleus began to separate until 4 min post-fertilization (mpf); both remained in a loose state at 6 mpf and started to condense at 8 mpf. This result indicates that 4–8 mpf may be the optimal initiation time. Approximately half of (47.74%±5.05%) the goldfish eggs developed into gynogenetic offspring when they were fertilized by UV-irradiated common carp sperm and treated with cold shock (0–2°C) for 30 min at 6 mpf (Figure 2C, Table S2 in Supporting Information).

To generate a truncated protein, a CRISPR/Cas9 target site of *lrp2aB* was chosen in the 8th exon (Figure 1E). To recreate the dragon-eye phenotype and other desirable traits in side-view goldfish, a Kirin Lion-head goldfish (♀) and a Black

Lion-head goldfish (♂) were selected as parents to produce diverse offspring. Half of the offspring were black and covered in normal scales, whereas the others displayed kirin, five-colored, and sakura patterns of coloration and were covered by transparent scales with a few normal scales (Figure S4 in Supporting Information). High concentrations of gRNA (200–300 pg) and Cas9 (800–1,000 pg) were co-injected into mature eggs before fertilization. Under the improved conditions for CRISPR/Cas9, a high proportion (>90.0%) of chimeric F0 individuals with mutated genotypes were generated. Of these, 12.2% exhibited chimeric phenotypes with enlarged eyes protruding from the eye sockets (Figure 1G).

Subsequently, an F0 Sakura female with a chimeric phenotype was selected to perform artificial gynogenesis. The F1 gynogenetic offspring were characterized by protuberant eyes that were morphologically similar to dragon-eye. The offspring were classified into two types according to coloration and scale pattern: black bodies with normal scales and white bodies with transparent scales. Ten individuals with protuberant eyes were arbitrarily sampled to investigate their genotypes; seven mutated genotypes were detected in which both alleles mutated into a premature stop codon (Figure S5 in Supporting Information). Importantly, some homozygous mutant individuals were generated through artificial gynogenesis, such as *lrp2aB*$^{-5/-5}$ (n=3) and *lrp2aB*$^{-4/-4}$ (n=2), which had truncated proteins composed of only 287 and 395 amino acids, respectively (Figure 1E, F).

As expected, the F1 gynogenetic offspring were all female when they were raised at a normal water temperature of 24°C. Fish sex differentiation depends on larval rearing temperature (Li and Gui, 2018; Li et al., 2018; Li et al., 2022). When they were raised for one month at a water temperature of 28°C from seven days after hatching, half of the F1 gynogenetic offspring reversed their sex from female to male. Consequently, a novel stable homozygous strain, which we call Black Dragon-eye Lion-head goldfish (Black Dragon-lion) (Figure 1G) was created by crossing F1 homozygous *lrp2aB*$^{-5/-5}$ mutant females and males (Figure 1E, F).

Similar to other Dragon-eye strains, the eyes of all edited *lrp2aB*$^{-5/-5}$ individuals began to protrude at approximately 60 days post-fertilization (dpf) and a complete morphological transformation was observed at about 90 dpf. Histological observation showed that the retinal layers became thinner and disordered (Figure S6 in Supporting Information), comparable to the defects observed in the Lrp2$^{G4469X/G4469X}$ Dragon-eye strain (Yu et al., 2021).

Therefore, *lrp2aB* is indeed the causal gene for the goldfish dragon-eye phenotype. Importantly, we recreated the dragon-eye phenotype in Lion-head goldfish that retained the preferred morphological traits of their parents, including a stout body with a lion-head phenotype and notably expanded and elongated double caudal fins, like a pleated skirt. Similarly, another novel stable homozygous strain, Jade Dragon-eye Lion-head goldfish (Jade Dragon-lion) (Figure 1G), was established via crossing F1 homozygous *lrp2aB*$^{-4/-4}$ mutant individuals (Figure 1E, F). The bodies of these offspring were white and covered by transparent scales, like jade. The dragon-eye, body color, and scale type phenotypes were stable in the Black Dragon-lion and Jade Dragon-lion strains, while only the thickness and pleat number of caudal fins showed subtle individual variations. And, all edited *lrp2aB*$^{-5/-5}$ or *lrp2aB*$^{-4/-4}$ individuals developed normally except for their eyes, indicating that the deficiency of Lrp2aB does not affect goldfish viability, growth, and reproduction. Additionally, a minor difference was observed between the edited and domesticated Dragon-eye mutants, in which a cataract symptom was observed from 22 months post-fertilization in the edited *lrp2aB*$^{-5/-5}$ or *lrp2aB*$^{-4/-4}$ mutant individuals, whereas similar symptom appeared until the two and a half years in the Lrp2$^{G4469X/G4469X}$ Dragon-eye strain (Figure S7 in Supporting Information).

Albino phenotype recreation

A previous study proposed that the albino phenotype might result from frameshift mutations in two homeologs of *oculocutaneous albinism type II* (*oca2*) (Kon et al., 2020). In this study, we recreated the albino phenotype in side-view goldfish by editing *oca2* genes. Oca2A and Oca2B (corresponding to Oca2S and Oca2L in Kon et al. (Kon et al., 2020), respectively) have 95.9% amino acid identity and both possess an important P_permease domain (Figure S8A in Supporting Information). To simultaneously generate three types of mutants (*oca2A*$^{-/-}$, *oca2B*$^{-/-}$, and *oca2A*$^{-/-}$;*oca2B*$^{-/-}$), the CRISPR/Cas9 target site was chosen in the conserved regions of *oca2A* and *oca2B* before the P_permease domain to completely disrupt these genes (Figure S8B in Supporting Information). The mating described above (Figure 1G, Figure S4 in Supporting Information) was used for the subsequent experiments.

In total, 15.3% of chimeric F0 individuals exhibited chimeric phenotypes with reduced or lost melanin (Figure 3A). The F1 gynogenetic offspring of an F0 chimeric female with tiger stripes displayed three phenotypes. The wild-type (WT) individuals (black body and black pupils, 27.6%±19.4%) all possessed at least one WT *oca2B* allele (Figure 3B). Complete disruption of Oca2A did not inhibit melanin synthesis in goldfish because some WT F1 gynogenetic offspring (70.0%) had two homozygous mutated *oca2A* alleles (Figure S9A in Supporting Information). Approximately 10% of offspring had gold bodies but their pupils were still black. Their genotypes were classified as *oca2A*$^{+/+}$;*oca2B*$^{-/-}$ and *oca2A*$^{+/-}$;*oca2B*$^{-/-}$ (Figure 3C) (Figure S9B in Supporting Information). The rest (62.2%±18.4%) were albino, with

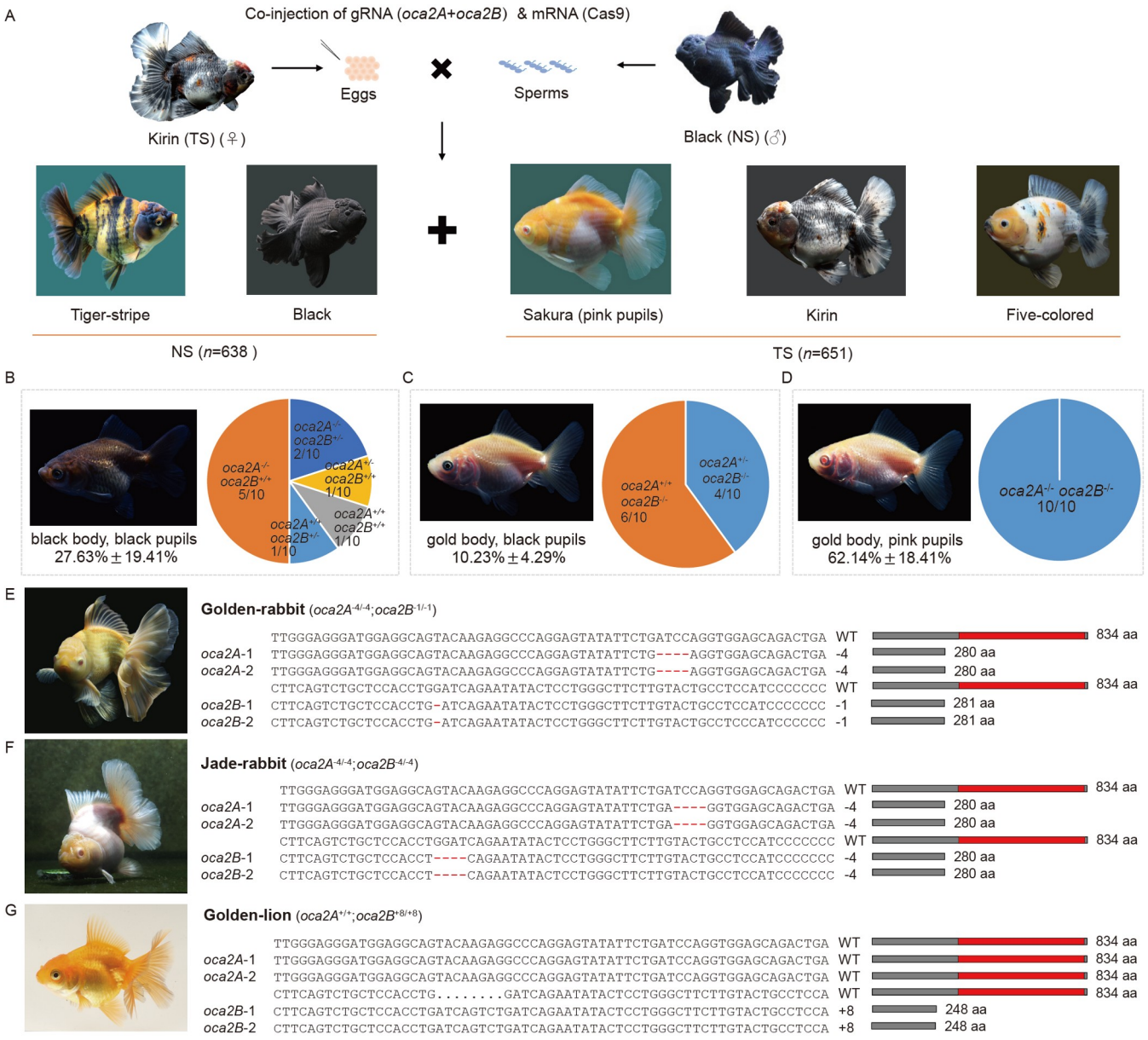

Figure 3 Recreation of the albino phenotype in side-view Lion-head goldfish. A, Morphology of the chimeric F0 mutant individuals. One F0 chimeric female with tiger stripes and one F0 female displaying the sakura pattern with pink pupils were selected to perform artificial meiotic gynogenesis. NS, normal scale; TS, transparent scale. B–D, Morphology and mutant genotypes of F1 gynogenetic mutant offspring. E–G, Morphology, edited genotype, and schematic representation of truncated proteins in Golden-rabbit, Jade-rabbit, and Golden-lion strains.

gold bodies and pink pupils, and all of them had the genotype *oca2A*$^{-/-}$;*oca2B*$^{-/-}$ (Figure 3D, Figure S9C in Supporting Information).

Some homozygous mutants, such as *oca2A*$^{-62/-62}$;*oca2B*$^{+/+}$ (n=3), *oca2A*$^{+/+}$;*oca2B*$^{+8/+8}$ (n=3), and *oca2A*$^{-4/-4}$;*oca2B*$^{-1/-1}$ (n=2), were generated through artificial gynogenesis (Figure S9 in Supporting Information). A novel stable strain, which we call the Albino Golden Pleated-skirt Lion-head (Golden-rabbit) goldfish, was created by crossing F1 homozygous *oca2A*$^{-4/-4}$;*oca2B*$^{-1/-1}$ mutant individuals. The individuals have a golden body, pink pupils, pleated skirt-like caudal fin, and head sarcoma (Figure 3E). Similarly, an F0 female individual displaying a sakura pattern with transparent scales and pink pupils, was selected to construct another F2 homozygous albino strain (*oca2A*$^{-4/-4}$;*oca2B*$^{-4/-4}$), Albino Jade-rabbit Pleated-skirt Lion-head goldfish (Jade-rabbit), which was named after a pet (jade rabbit) in Chinese mythology that lives on the moon with the fairy Chang'e (Figure 3F). Under careful raising in the laboratory, all edited *oca2A*$^{-4/-4}$;*oca2B*$^{-1/-1}$ and *oca2A*$^{-4/-4}$;*oca2B*$^{-4/-4}$ individuals developed normally. In addition, a mutant strain (*oca2A*$^{+/+}$;*oca2B*$^{+8/+8}$) with a golden body and black pupils was generated and called Golden Pleated-skirt Lion-head goldfish (Golden-lion) (Figure 3G).

Subfunctionalization of oca2A and oca2B

To explore the function of the divergence between *oca2A* and *oca2B*, the morphology of scales and histological structure of eyes were compared among WT, Golden-lion, Golden-rabbit, and Jade-rabbit goldfish. Relative to WT with normal scales, the coloration of the Golden-lion goldfish was similar to that of the WT goldfish during embryogenesis and the juvenile stage, but their bodies began to depigment at two months after hatching (Figure 4A). After two months, the bodies of Golden-lion goldfish became golden and the pigment granules completely vanished from their scales (Figure 4B). Consistent with depigmentation of the body surface, melanin granules also gradually faded in the iris and choroid but were unaffected in the retinal pigment epithelia (RPE) of the eyes (Figure 4C). By contrast, melanogenesis was completely inhibited throughout Golden-rabbit goldfish development, including in the skin, scale, iris, choroidal melanocytes, and RPE (Figure 4A–C). In addition, Jade-rabbit goldfish were transparent and absolutely lost melanin throughout the body and reflecting platelets in scales (Figure 4A–C).

To reveal the link between *oca2* homeologs and body color changes, we analyzed *oca2A* and *oca2B* expression in the

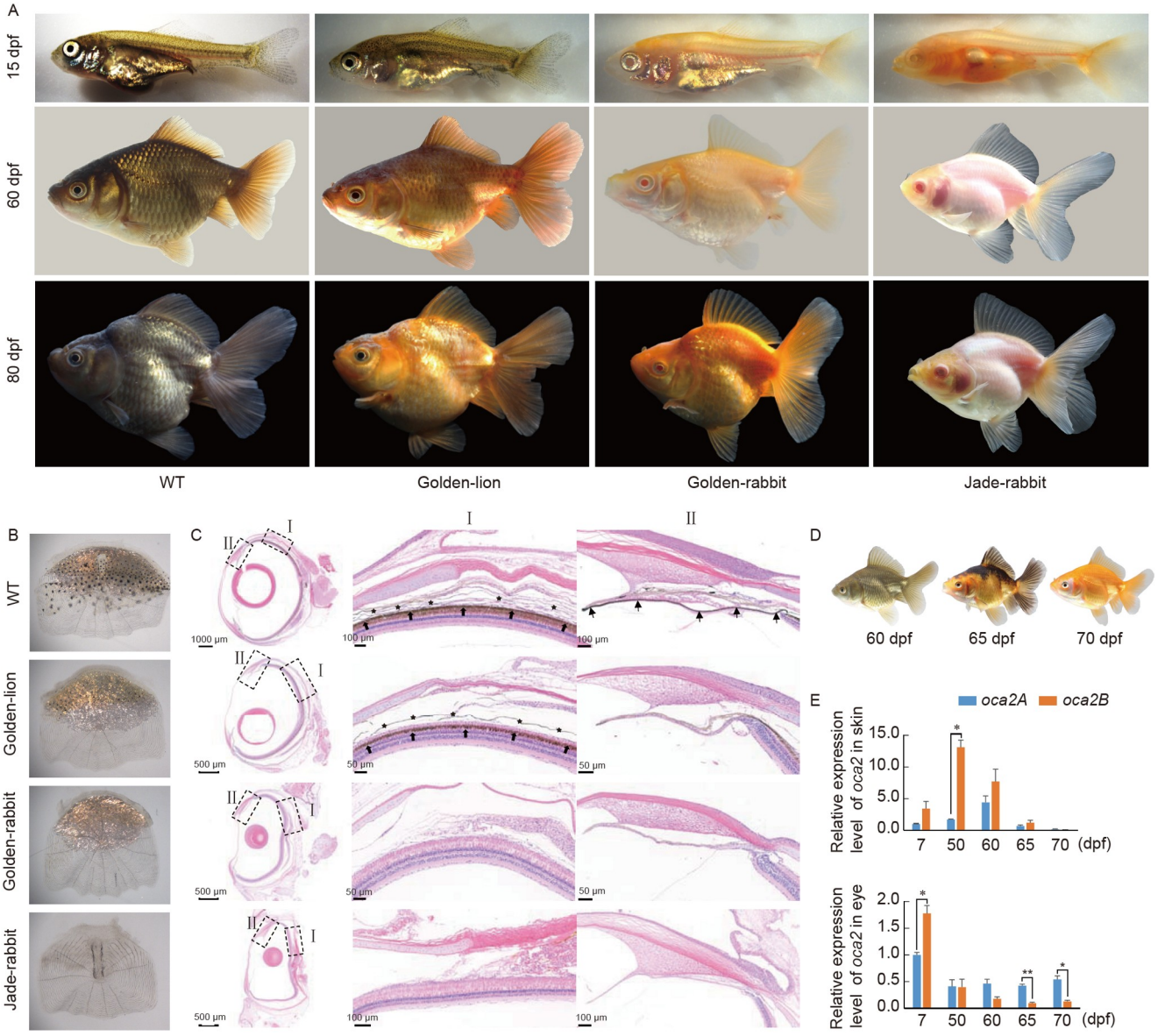

Figure 4 *oca2A* and *oca2B* cooperatively regulate melanogenesis in goldfish. A, Fish morphology of WT and three *oca2* mutant strains at different developmental stages. B, Scale morphology. C, Transverse section of eyes stained with hematoxylin and eosin. Scale bars are shown in the lower left of each picture. Melanin granules in the RPE, iris, and choroid are indicated by thick arrows, thin arrows, and stars, respectively. D, Depigmentation process in Red-white Lion-head goldfish. E, qPCR analyses of *oca2A* and *oca2B* in skin and eyes. *β-actin* was used to normalize data. Gene expression levels are shown relative to that of *oca2A* in skin. Each bar represents the mean±SD (n=3). *, P<0.05, **, P<0.01.

skin and eyes of Red-white Lion-head goldfish in which body surface depigmented at two months post-hatching (Figure 4D), similar to Golden-lion goldfish. Consistent with the dominant role of *oca2B* in melanogenesis of the body surface, *oca2B* was more highly expressed in skin than *oca2A* (Figure 4E). Because normal melanogenesis occurs in Golden-lion goldfish before depigmentation, we suggest that the lower expression of *oca2A* during early development is sufficient for initial melanogenesis. Accompanied by depigmentation, both *oca2A* and *oca2B* exhibited gradually decreased expression in skin (Figure 4E). Even though *oca2A* and *oca2B* expression reduces in eyes during development, *oca2A* maintains relatively stable expression compared with *oca2B*, and more *oca2A* transcripts were detected from 70 dpf (Figure 4E). The data indicate that subfunctionalization of *oca2A* and *oca2B* has evolved in goldfish.

Creation of more appealing goldfish

Using the past conventional breeding strategy (Figure 5A), diverse offspring are produced when two different goldfish strains, such as Pleated-skirt Lion-head goldfish and Dragon-eye Butterfly goldfish, are hybridized. It would need to take 7–10 generations to selectively breed a relatively stable strain that integrates the dragon-eye phenotype inherited from Dragon-eye Butterfly goldfish and most of the superior traits such as body size, tail extension, and head sarcoma inherited from Plead-skirt lion-head goldfish. Nonetheless, some traits still exhibit phenotypic variations among individuals of the offspring. In this study, we developed a rapid and precise biotechnology approach to create novel appealing goldfish strains within two generations (approximately eight months) (Figure 5B).

By the precise breeding, we produced four stable homozygous goldfish strains: Black Dragon-lion (*lrp2aB*$^{-5/-5}$) (Figure 5C), Jade Dragon-lion (*lrp2aB*$^{-4/-4}$) (Figure 5D), Golden-rabbit (*oca2A*$^{-4/-4}$;*oca2B*$^{-1/-1}$) (Figure 5E), and Jade-rabbit (*oca2A*$^{-4/-4}$;*oca2B*$^{-4/-4}$) (Figure 5F). The individuals of each strain displayed almost identical morphology. Approximately one century ago, Shisan C. Chen discussed the presence of transparent scales, which is a dominant trait, as the first case of Mendelian inheritance in goldfish (Chen, 1928). Even though the causal gene associated with transparent scales has not yet been identified, we were able to use this trait to create more colorful goldfish by hybridizing edited strains with normal and transparent scales. For example, Kirin Dragon-lion, Sakura Dragon-lion, Five-colored Dragon-lion, and Dairy-cattle Dragon-lion (*lrp2aA*$^{-5/-4}$) goldfish (Figure 5G) were produced when Black Dragon-lion goldfish (*lrp2aA*$^{-5/-5}$) were mated with Jade Dragon-lion goldfish (*lrp2aA*$^{-4/-4}$). Similarly, Sakura Jade-rabbit goldfish with pink pupils (*oca2A*$^{-4/-4}$;*oca2B*$^{-1/-4}$) (Figure 5H) were produced when Golden-rabbit goldfish (*oca2A*$^{-4/-4}$;*oca2B*$^{-1/-1}$) were mated with Jade-rabbit goldfish (*oca2A*$^{-4/-4}$;*oca2B*$^{-4/-4}$). In addition, some F0 chimeric individuals with high ornamental value, such as Tiger-stripe goldfish (Figure 5I), were also generated.

DISCUSSION

"With the most extraordinary modifications of structure" (Darwin, 1868), the genetic basis of goldfish morphological diversity has long fascinated evolutionary biologists and geneticists (Gui et al., 2022; Zhou and Gui, 2017). Recently, Kon et al. (Kon et al., 2020) provided a clue to explore the mystery. In this study, we developed a rapid biotechnology approach to construct homozygous goldfish knockout strains, and confirmed that *lrp2aB* and two *oca2* homeologs are required for dragon-eye and albino morphogenesis, respectively. Moreover, we found that the subfunctionalization of *oca2A* and *oca2B* lead to differential melanogenesis in the body surface and pupils of goldfish.

Several phenotypic variations, including dragon-eye and albino phenotypes, have been thought to be determined by single major-effect loci (Kon et al., 2020). However, there are few functional verification reports, probably because it is difficult to edit genes in allotetraploid goldfish and it is inconvenient to obtain fertilized eggs as a result of the one-year sexual maturation cycle and seasonal spawning of goldfish. In this study, we improved the conditions for breeding, gene editing, artificial gynogenesis, and temperature-induced sex reversal. Then, we combined these approaches to recreate goldfish homozygous mutants within two generations (approximately eight months), which is similar in efficiency to zebrafish. Then, we confirmed that *lrp2aB* and two *oca2* homeologs were indeed the causal genes associated with dragon-eye and albino phenotypes, respectively. Importantly, our study provides an efficient approach to rapidly recreate desirable phenotype in goldfish, referring as re-domestication (Hanak et al., 2022), and even by *de novo* domestication from wild *C. auratus*.

C. auratus, including the domesticated goldfish, descended from an allotetraploidy event. As an amphidiploid, it had been revealed to experience diploidization (Lin and Mei, 2022; Lu et al., 2021; Wang et al., 2022b). It was reported that the two subgenomes of goldfish have probably functionally diverged (Chen et al., 2020; Kon et al., 2020; Luo et al., 2020; Wang et al., 2022b), which was thought to possibly contribute to the generation of diverse morphological variations in goldfish (Kon et al., 2020). The significance and implications of whole-genome duplication (WGD) for trait innovations, ecological adaptation, and speciation and diversification have been extensively discussed (Cheng et al., 2018, Fox et al., 2020, Soltis and Soltis, 2016; Van de Peer et

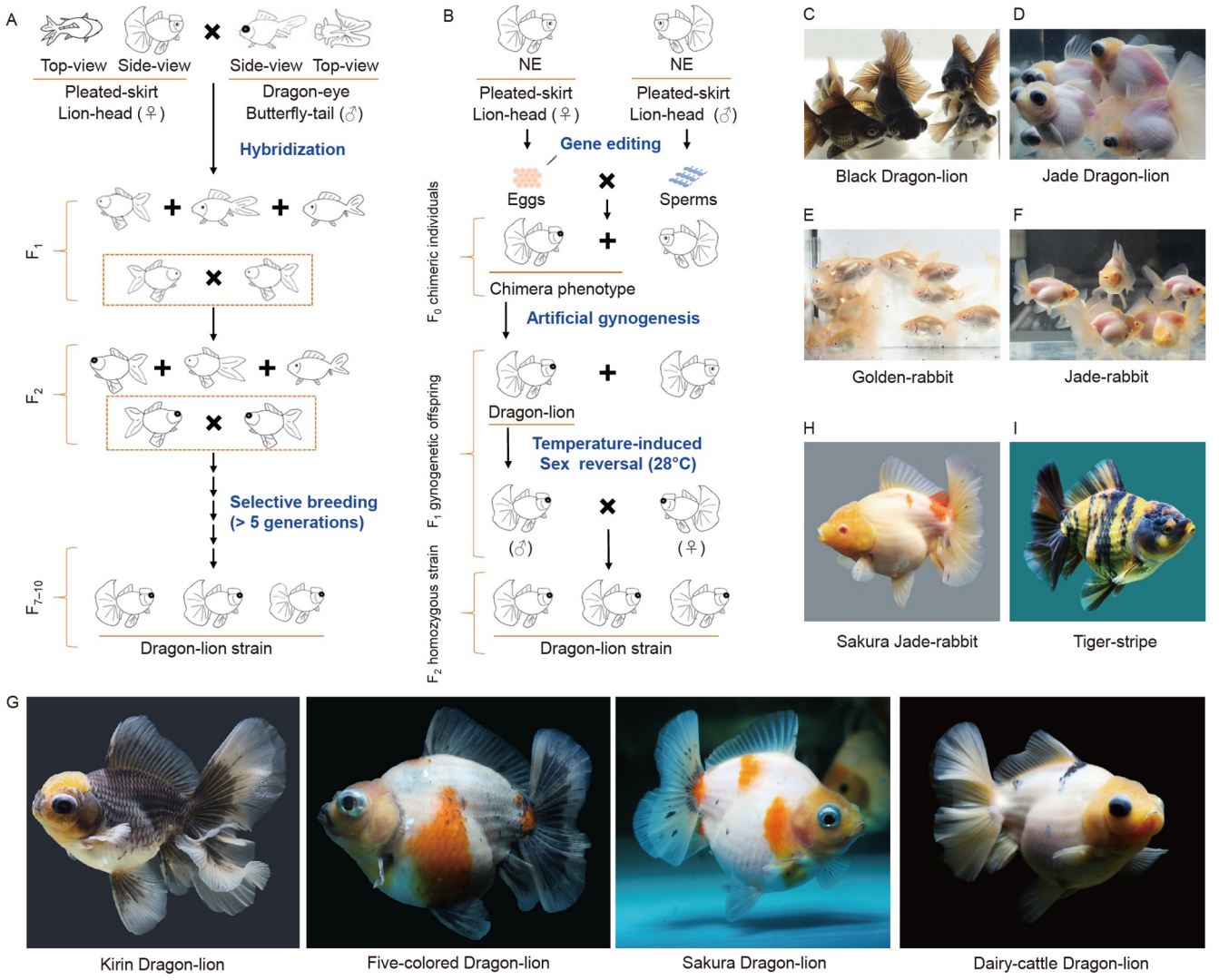

Figure 5 Flowchart and establishment of six novel goldfish strains. A, Flowchart of the conventional strategy via hybridization and selective breeding. Breeding of Pleated-skirt Dragon-eye Lion-head goldfish by crossing Pleated-skirt Lion-head goldfish and Dragon-eye Butterfly-tail goldfish was taken as an example. B, Flowchart of the novel breeding approach that combines gene editing, high-efficiency breeding, artificial gynogenesis, and temperature-induced sex reversal. C–F, Morphology of four homozygous mutated strains, including Black Dragon-lion (C), Jade Dragon-lion (D), Golden-rabbit (E), and Jade-rabbit (F). G, Morphology of offspring produced by mating Jade Dragon-lion goldfish with Black Dragon-lion goldfish. H, Morphology of Sakura Jade-rabbit produced by mating Golden-rabbit goldfish with Jade-rabbit goldfish. I, Morphology of an F0 chimeric individual with the tiger-stripe phenotype.

al., 2017; Zhou and Gui, 2017). After WGD, one of the two duplicated genes may be deleted or pseudogenized to lose function, subfunctionalized to retain the partial function of the ancestral gene, or neofunctionalized to evolve a novel function (Cheng et al., 2018). Recently, we assembled the genomes of goldfish (*C. auratus*) and gibel carp (*C. gibelio*) and demonstrated that goldfish are amphidiploid and *C. gibelio* are an amphitriploid (AAABBB) that originated from a common ancestor of *C. auratus* and experienced an extra autotriploidy event (Wang et al., 2022b). We also elucidated the subfunctionalization and neofunctionalization of multiple duplicated *foxl2*, *viperin*, *ptpn6*, and *gsdf* homeologs/alleles in *C. gibelio* (Gan et al., 2021; Mou et al., 2022; Tong et al., 2021; Wang et al., 2022a).

The goldfish *lrp2a* homeolog seems to have been lost from the A subgenome (corresponding to the S subgenome in Kon et al. (Kon et al., 2020)), and only one homeolog (*lrp2aB* or *lrp2aL*) was screened in the four assembled *C. auratus* genomes. Lrp2a, as a multifunctional endocytic receptor, plays pivotal but complex intertwined functions in lipid metabolism and some morphogen signaling (Christ et al., 2016). In humans, several mutations in LRP2 have been suggested to be associated with Donnai-Barrow syndrome, a rare disease characterized by enlarged eye globes and high myopia (Kantarci et al., 2007). The *bugeye* (buphthalmia) phenotype in zebrafish is most likely caused by a single recessive mutation (C23X or Q413X) in Lrp2 (Veth et al., 2011), and homozygous Lrp2$^{S4424NX/S4424NX}$ zebrafish also have the phenotype of enlarged eyes observed in *bugeye* zebrafish (Collery and Link, 2019). Consistent with its

mammalian and zebrafish homologs (Saito et al., 1994), goldfish WT Lrp2aB protein is predicted to be composed of a large N-terminal extracellular region, a single transmembrane domain, and a short C-terminal cytoplasmic tail. In this study, we first identified a mutation (G4469X) in the Dragon-eye strain Lrp2$^{G4469X/G4469X}$ (Figure 1D, E) and Butterfly Moor goldfish (Figure S3 in Supporting Information), which resulted in the complete loss of the two NPXY motifs within the cytoplasmic tail (Figure 1F). The same stop codon mutation was previously identified in Black Telescope-eye and Albino Celestial strains (Kon et al., 2020). The NPXY motif has been shown to be the binding site for cytoplasmic adaptor proteins that are involved in clathrin-coated endocytosis (Chen et al., 1990; Christensen and Birn, 2002). Therefore, the absence of the NPXY motif may disrupt the normal function of Lrp2aB acting as endocytic receptor. Subsequently, we generated two goldfish mutant lines (*lrp2aB*$^{-5/-5}$ and *lrp2aB*$^{-4/-4}$) that were predicted to express only a partial N-terminal extracellular region. They both had enlarged eye globes (Figure 1G).

In *Lrp2*$^{-/-}$ mice, Lrp2 deficiency induces sonic hedgehog (SHH)-dependent hyperproliferation of cells in the ciliary marginal zone, which may cause the large eye phenotype (Christ et al., 2015). Moreover, cholesterol is essential for SHH signaling activation (Radhakrishnan et al., 2020). *lrp2* is known to be expressed in RPE and ciliary epithelium (Storm et al., 2014; Veth et al., 2011), which indicates that it has pivotal roles in nutrient transport across the blood-retinal and blood-aqueous humour barriers (Ramachandra Rao and Fliesler, 2021). The disruption of goldfish Lrp2aB function results in the dysregulation of lipid homeostasis (Yu et al., 2021), which may in turn affect eye morphogenesis and retinal cytoarchitecture. In this study, we also observed a subtle time difference in the cataract appearance between the edited *lrp2aB*$^{-5/-5}$ or *lrp2aB*$^{-4/-4}$ mutant and the domesticated Lrp2$^{G4469X/G4469X}$ Dragon-eye mutant (Figure S7 in Supporting Information), implying that the disruption of most domains of Lrp2aB might have more serious effects than that induced by the absence of NPXY motif. Of course, there is still much to study on this topic, including performing a complementarity assay to determine that the dragon-eye phenotype in the domesticated strain is indeed caused by the G4469X mutation in Lrp2aB, and thereby analyzing the reason for the time difference of the cataract appearance. And, the interactions among lipid homeostasis, morphogen signaling, and eye morphogenesis intertwined by Lrp2aB still need to be elucidated.

The evolutionary fate of *oca2* is another scenario. Both homeologs of *oca2* have been retained in goldfish but their functions have diverged. Consistent with the human (*Homo sapiens*) Oca2 disease phenotype (Suzuki and Tomita, 2008), *oca2* mutants of several animal models, such as mice (*Mus musculus*) (Johnson et al., 1995), zebrafish (*Danio rerio*) (Beirl et al., 2014), medaka (*Oryzias latipes*) (Fukamachi et al., 2004), and Mexican cave tetra (*Astyanax mexicanus*) (Protas et al., 2006), all display hypopigmentation of skin and RPE; this indicates a conserved role of *oca2* in melanophore differentiation and melanin synthesis. After allotetraploidization, goldfish *oca2A* and *oca2B* have subfunctionalized to synergistically but differentially govern melanogenesis in the goldfish body surface and eyes. *oca2B* plays a dominant role in goldfish melanin synthesis because the individuals with even one WT *oca2B* allele all displayed normal body coloration and black pupils. By contrast, *oca2A* is independently capable of determining normal melanogenesis in melanophores during early development but cannot maintain its function; pigment granules gradually fade in these cells from *oca2A*$^{+/+}$;*oca2B*$^{-/-}$ goldfish at two months after hatching. Interestingly, we also observed similar dynamic changes of iris and choroid pigment granules but unaffected melanogenesis in RPE of *oca2A*$^{+/+}$;*oca2B*$^{-/-}$. This is possible because iris and choroidal melanocytes are also neural crest-derived cells, similar to melanophores in the body surface, whereas RPE originates from optic neuroepithelium (Lister, 2002). Therefore, there are overlapping functions of *oca2A* and *oca2B* in melanogenesis in RPE but only *oca2B* retains all of its conserved function in melanophores and melanocytes derived from neural crest cells.

In conclusion, we recreated dragon-eye and albino phenotypes in goldfish by editing the causal *lrp2aB* and two *oca2* homeologs, respectively. Then, we created four stable homozygous strains and more appealing goldfish with desirable traits. The precise genetic breeding approach used in our study will accelerate re-domestication and recreation of more aesthetically appealing goldfish.

MATERIALS AND METHODS

Goldfish culture and propagation

Goldfish were raised in fish tanks at the National Aquatic Biological Resource Center (NABRC). As the goldfish grew, they were sequentially fed live nauplii hatched from the eggs of brine shrimp, water angleworms, frozen chironomid larvae, and commercial feed (51% protein, 10% fat, 2% fiber) (Table S1 in Supporting Information). Fish tanks were equipped with a filtration system to reduce the ammonia nitrogen and nitrite content. Under improved raising conditions, goldfish had a 1:1 sex ratio. For the temperature-induced sex reversal experiment, goldfish fries (< 2 cm) were raised for one month at a water temperature of 28°C from seven days after hatching.

After 90 dpf, healthy goldfish were chosen to perform propagation experiments. Generally, three females and two males were cultured in a fish tank (250 L). When the males were chasing the females or a few eggs were found at the

bottom of fish tank, females were caught to squeeze eggs into a 10-mL tube for subsequent experiments. After propagation, postpartum care was performed, including exchanging a quarter of the water and replacing the filter cotton. When necessary, 1‰–2‰ salt was added to the water to ensure the fish were healthy (Brown et al., 2018; Miron et al., 2003).

WGR-based BSA

WGR-based BSA was performed in one F3 segregated population from a Dragon-eye strain (Figure S1 in Supporting Information) and their parents. As shown in Figure S2 in Supporting Information, two DNA bulks from 30 normal-eyed offspring, 30 dragon-eyed offspring, and their parents (30× genomic coverage) were sequenced (average coverage, 1× per individual) using an Illumina HiSeq XTen PE150 platform. Raw reads were filtered using SOAPnuke 1.5.5 (Chen et al., 2018) (Table S3 in Supporting Information). In total, 52.18 Gb clean reads with Q30 ≥ 92.08% (Table S3 in Supporting Information) were mapped to the reference genome of crucian carp (*C. auratus*) (Wang et al., 2022b) using BWA 0.7.12 (Li and Durbin, 2009) (Table S4 in Supporting Information), followed by SNP calling using GATK 3.36 (Li et al., 2009), which resulted in 14,873,974–17,128,867 SNPs called from the four sequenced samples (Table S5 in Supporting Information).

Then, the SNPs were processed to identify candidate genes. First, SNPs were removed that were absent from the parents or the two DNA bulks of offspring with depth < 8 and genotype quality < 20. Second, SNPs were retained in which the paternal dragon-eyed parent (♂) was homozygous but the maternal normal-eyed parent (♀) was heterozygous. Third, the SNP index (the ratio of non-reference reads to the total reads mapped to the variation site) was calculated for the two DNA bulks using the SNPs in the paternal dragon-eyed parent (♂) as the reference genotype; SNPs were called if they had an SNP index of approximately 0 for dragon-eyed goldfish and approximately 0.5 for normal-eyed goldfish. Fourth, the average negative logarithmic *P*-values of SNPs were smoothed by a sliding window (size=100 kb, step=10 kb) across each chromosome of the *C. auratus* assembled genome, and six candidate regions (containing 201 genes, Table S6 in Supporting Information) were determined with confidence intervals of 95%. Finally, SNPs were called in the start/stop codon of genes that were differentially expressed between normal-eyed and dragon-eyed goldfish (FPKM > 1) (Yu et al., 2021).

Optimal conditions of artificial meiotic gynogenesis

UV irradiation and cold shock were performed to induce genetic inactivation and chromosome diploidy, respectively. The hybrids of goldfish and common carp show obvious morphological differences from their parents. Thus, UV-irradiated common carp sperm was used as a trigger to activate embryogenesis. Briefly, 300 μL sperm of common carp was diluted using 7 mL sperm preservation solution (Li et al., 2020) and evenly spread on a Petri dish (100 mm in diameter). The UV irradiation dose was 300 μW cm^{-2} and the distance between the Petri dish and UV lamp was 18 cm. UV irradiation for 10 min enabled common carp sperm to be genetically inactivated and no hybrid individual was observed in the offspring. The goldfish eggs were fertilized by UV-irradiated common carp sperm at 24°C. Then, the fertilized eggs were treated by cold shock (0–2°C) for 30 min at 2, 4, 6, 8, and 9 min post-fertilization. The control group included goldfish eggs fertilized by homologous sperm without any treatment. The fertilization rate, hatching rate, and survival rate of embryos or fries were determined at 13 h post-fertilization (gastrula stage), 100 h post-fertilization (hatching stage), and 7 days post-hatching.

All groups were incubated in the hatching water (20–24°C). The fertilized eggs at 2, 3, 4, 6, 8, and 9 min post-fertilization were fixed by 4% paraformaldehyde and stained with 4′,6-diamidino-2-phenylindole (DAPI) (Sigma, St Louis, MO, USA) as previously described (Wang et al., 2021; Zhao et al., 2021). Stacked images acquired under a Leica SP8 DLS confocal microscope (Analytical & Testing Center, Institute of Hydrobiology, Chinese Academy of Sciences, Wuhan, China) were used to render the 3D reconstructions of the male pronucleus, female pronucleus, and second polar body.

Generation of goldfish homozygous mutants

The DNA sequences of goldfish *lrp2aB*, *oca2A*, and *oca2B* were downloaded from Ensembl (http://www.ensembl.org/index.html). CRISPR/Cas9 gene editing was performed as previously described (Gan et al., 2021). First, 200–300 pg sgRNA and 800–1,000 pg Cas9 were co-injected into the eggs of normal-scaled Pleated-skirt Lion-head goldfish. The eggs were left at room temperature for 10 min and then fertilized by the sperm of normal-scaled pleated-skirt lion-head goldfish. Total DNA was extracted using the Ezup Column Animal Genomic DNA Kit (Sangon, Shanghai, China). The mutations were analyzed by PCR using Rapid Taq Master Mix (Vazyme, Nanjing, China) and sequenced by Quintarabio (Wuhan, China).

F0 goldfish with chimeric dragon-eye or albino phenotypes were selected for artificial gynogenesis to obtain F1 homozygous mutants. Half of the F1 larvae were raised at 28°C for 30 days after hatching to reverse the sex of some females into males. Then, numerous homozygous mutants were produced by crossing the F1 females and males with the same mutant genotype.

Eye histopathology, scale microscopic examination, and qPCR analysis

WT and mutant eyes were fixed in 4% paraformaldehyde overnight at 4°C. After being dehydrated and embedded, samples were cut into 4 μm sections and stained with hematoxylin and eosin (Pinuofei, Servivebio, Wuhan, China). Bright-field images of eye structure were captured via a 3D Panoramic 250 scanner (3DHISTECH, Budapest, Hungary) using CaseViewer 2.4. The bright-field images of scales were captured via a Stemi 508 stereo microscope (Zeiss, Oberkochen, Germany) using uScope Essntials 22.5.

The skin and eyes of Red-white Lion-head goldfish at 5, 50, 70, 75, and 80 dpf (n=3) were used to perform qPCR as previously described (Yu et al., 2021). The primers are listed in Table S7 in Supporting Information. *β-actin* was used to normalize qPCR data. The relative expression levels were calculated using the $2^{-\Delta\Delta Ct}$ method, and Tukey's test was conducted in SPSS 22.0 for statistical analysis.

Data availability

Data supporting these findings are available in the paper and Supplementary Information.

Compliance and ethics *The author(s) declare that they have no competing interest.*

Acknowledgements *This work was supported by the National Key Research and Development Program of China (2018YFD0901202), the Strategic Priority Research Program of Chinese Academy of Sciences (XDB31000000), the Knowledge Innovation Program of Wuhan -Basic Research (2022020801010143), the Autonomous Project of the State Key Laboratory of Freshwater Ecology and Biotechnology (2021FB02), and the China Agriculture Research System of MOF and MARA. The research was supported by the Wuhan Branch, Supercomputing Center, Chinese Academy of Sciences, China. We thank Fang Zhou for providing confocal services (Analytical & Testing Center, Institute of Hydrobiology, Chinese Academy of Sciences). We thank Mallory Eckstut, PhD for editing the English text of a draft of this manuscript.*

References

Abdelrahman, H., ElHady, M., Alcivar-Warren, A., Allen, S., Al-Tobasei, R., Bao, L., Beck, B., Blackburn, H., Bosworth, B., Buchanan, J., et al. (2017). Aquaculture genomics, genetics and breeding in the united states: current status, challenges, and priorities for future research. BMC Genomics 18, 191.

Beirl, A.J., Linbo, T.H., Cobb, M.J., and Cooper, C.D. (2014). *oca2* regulation of chromatophore differentiation and number is cell type specific in zebrafish. Pigment Cell Melanoma Res 27, 178–189.

Brown, C., Wolfenden, D., and Sneddon, L. (2018). Goldfish (*Carassius auratus*). In: Yeates, J., ed. Companion Animal Care and Welfare: The UFAW Companion Animal Handbook. Sussex: John Wiley & Sons. 467–478.

Chen, D., Zhang, Q., Tang, W., Huang, Z., Wang, G., Wang, Y., Shi, J., Xu, H., Lin, L., Li, Z., et al. (2020). The evolutionary origin and domestication history of goldfish (*Carassius auratus*). Proc Natl Acad Sci USA 117, 29775–29785.

Chen, S.C. (1928). Transparency and mottling, a case of Mendelian inheritance in the goldfish *Carassius auratus*. Genetics 13, 434–452.

Chen, S.C. (1954). History of the domestication and the factors of the varietal formation of the common goldfish, *Carassius auratus*. Sci Sin Vitae 5, 287–321.

Chen, W.J., Goldstein, J.L., and Brown, M.S. (1990). NPXY, a sequence often found in cytoplasmic tails, is required for coated pit-mediated internalization of the low density lipoprotein receptor. J Biol Chem 265, 3116–3123.

Chen, Y., Chen, Y., Shi, C., Huang, Z., Zhang, Y., Li, S., Li, Y., Ye, J., Yu, C., Li, Z., et al. (2018). SOAPnuke: a MapReduce acceleration-supported software for integrated quality control and preprocessing of high-throughput sequencing data. GigaScience 7, gix120.

Cheng, F., Wu, J., Cai, X., Liang, J., Freeling, M., and Wang, X. (2018). Gene retention, fractionation and subgenome differences in polyploid plants. Nat Plants 4, 258–268.

Christ, A., Christa, A., Klippert, J., Eule, J.C., Bachmann, S., Wallace, V. A., Hammes, A., and Willnow, T.E. (2015). LRP2 acts as SHH clearance receptor to protect the retinal margin from mitogenic stimuli. Dev Cell 35, 36–48.

Christ, A., Herzog, K., and Willnow, T.E. (2016). LRP2, an auxiliary receptor that controls sonic hedgehog signaling in development and disease. Dev Dyn 245, 569–579.

Christensen, E.I., and Birn, H. (2002). Megalin and cubilin: multifunctional endocytic receptors. Nat Rev Mol Cell Biol 3, 258–267.

Collery, R.F., and Link, B.A. (2019). Precise short sequence insertion in zebrafish using a CRISPR/Cas9 approach to generate a constitutively soluble Lrp2 protein. Front Cell Dev Biol 7, 167.

Darwin, C.R. (1868). Duck goose peacock turkey guinea fowl canary bird goldfish hive bees silk moths. In: Darwin C.R, ed. The Variation of Animals and Plants under Domestication. London: John Murray. 296–313.

Fox, D.T., Soltis, D.E., Soltis, P.S., Ashman, T.L., and Van de Peer, Y. (2020). Polyploidy: a biological force from cells to ecosystems. Trends Cell Biol 30, 688–694.

Fukamachi, S., Asakawa, S., Wakamatsu, Y., Shimizu, N., Mitani, H., and Shima, A. (2004). Conserved function of medaka pink-eyed dilution in melanin synthesis and its divergent transcriptional regulation in gonads among vertebrates. Genetics 168, 1519–1527.

Gan, R.H., Wang, Y., Li, Z., Yu, Z.X., Li, X.Y., Tong, J.F., Wang, Z.W., Zhang, X.J., Zhou, L., and Gui, J.F. (2021). Functional divergence of multiple duplicated *Foxl2* homeologs and alleles in a recurrent polyploid fish. Mol Biol Evol 38, 1995–2013.

Gratacap, R.L., Wargelius, A., Edvardsen, R.B., and Houston, R.D. (2019). Potential of genome editing to improve aquaculture breeding and production. Trends Genet 35, 672–684.

Gui, J.F., Zhou, L., and Li, X.Y. (2022). Rethinking fish biology and biotechnologies in the challenge era for burgeoning genome resources and strengthening food security. Water Biol Security 1, 100002.

Hanak, T., Madsen, C.K., and Brinch-Pedersen, H. (2022). Genome Editing-accelerated Re-Domestication (GEaReD)—a new major direction in plant breeding. Biotechnol J 17, 2100545.

Houston, R.D., Bean, T.P., Macqueen, D.J., Gundappa, M.K., Jin, Y.H., Jenkins, T.L., Selly, S.L.C., Martin, S.A.M., Stevens, J.R., Santos, E.M., et al. (2020). Harnessing genomics to fast-track genetic improvement in aquaculture. Nat Rev Genet 21, 389–409.

Johnson, D.K., Stubbs, L.J., Culiat, C.T., Montgomery, C.S., Russell, L.B., and Rinchik, E.M. (1995). Molecular analysis of 36 mutations at the mouse pink-eyed dilution (p) locus. Genetics 141, 1563–1571.

Kantarci, S., Al-Gazali, L., Hill, R.S., Donnai, D., Black, G.C.M., Bieth, E., Chassaing, N., Lacombe, D., Devriendt, K., Teebi, A., et al. (2007). Mutations in *LRP2*, which encodes the multiligand receptor megalin, cause donnai-barrow and facio-oculo-acoustico-renal syndromes. Nat Genet 39, 957–959.

Kon, T., Omori, Y., Fukuta, K., Wada, H., Watanabe, M., Chen, Z., Iwasaki, M., Mishina, T., Matsuzaki, S.I.S., Yoshihara, D., et al. (2020). The genetic basis of morphological diversity in domesticated goldfish. Curr

Biol 30, 2260–2274.e6.
Li, H., and Durbin, R. (2009). Fast and accurate short read alignment with burrows-wheeler transform. Bioinformatics 25, 1754–1760.
Li, H., Handsaker, B., Wysoker, A., Fennell, T., Ruan, J., Homer, N., Marth, G., Abecasis, G., and Durbin, R. (2009). The sequence alignment/map format and samtools. Bioinformatics 25, 2078–2079.
Li, X.Y., and Gui, J.F. (2018). Diverse and variable sex determination mechanisms in vertebrates. Sci China Life Sci 61, 1503–1514.
Li, X.Y., Liu, X.L., Zhu, Y.J., Zhang, J., Ding, M., Wang, M.T., Wang, Z. W., Li, Z., Zhang, X.J., Zhou, L., et al. (2018). Origin and transition of sex determination mechanisms in a gynogenetic hexaploid fish. Heredity 121, 64–74.
Li, X.Y., Mei, J., Ge, C.T., Liu, X.L., and Gui, J.F. (2022). Sex determination mechanisms and sex control approaches in aquaculture animals. Sci China Life Sci 65, 1091–1122.
Li, Z., Lu, M., Wang, Z.W., Li, X.Y., Wang, Y., Zhang, X.J., and Gui, J.F. (2020). An effective method for creating allo-octoploids by integrating exogenous sperm genome into gibel carp eggs (in Chinese). Acta Hydrobiol Sin 44, 26–35.
Lin, Q., and Mei, J. (2022). Genomic characterization of an amphitriploid fish and insights into the evolutionary mechanisms of unisexual reproduction success. Water Biol Security 1, 100066.
Lister, J.A. (2002). Development of pigment cells in the zebrafish embryo. Microsc Res Tech 58, 435–441.
Lu, M., Li, X.Y., Li, Z., Du, W.X., Zhou, L., Wang, Y., Zhang, X.J., Wang, Z.W., and Gui, J.F. (2021). Regain of sex determination system and sexual reproduction ability in a synthetic octoploid male fish. Sci China Life Sci 64, 77–87.
Luo, J., Chai, J., Wen, Y., Tao, M., Lin, G., Liu, X., Ren, L., Chen, Z., Wu, S., Li, S., et al. (2020). From asymmetrical to balanced genomic diversification during rediploidization: subgenomic evolution in allotetraploid fish. Sci Adv 6, eaaz7677.
Miron, D.S., Silva, L.V.F., Golombieski, J.I., and Baldisserotto, B. (2003). Efficacy of different salt (NaCl) concentrations in the treatment of *Ichthyophthirius multifiliis-Infected* silver catfish, *Rhamdia quelen*, fingerlings. J Appl Aquacul 14, 155–161.
Mou, C.Y., Wang, Y., Yu, P., Li, Z., Wang, Z.W., Li, X.Y., Li, S., Lu, L.F., Tong, J.F., Zhang, Q.Y., et al. (2022). Cooperative antivirus activities of two duplicated viperin homeologs confirmed by CRISPR/Cas9 editing in hexaploid gibel carp. Aquaculture 548, 737609.
Nie, C.H., Wan, S.M., Chen, Y.L., Huysseune, A., Wu, Y.M., Zhou, J.J., Hilsdorf, A.W.S., Wang, W., Witten, P.E., Lin, Q., et al. (2022). Single-cell transcriptomes and *runx2b*$^{-/-}$ mutants reveal the genetic signatures of intermuscular bone formation in zebrafish. Natl Sci Rev, doi: 10.1093/nsr/nwac152.
Okoli, A.S., Blix, T., Myhr, A.I., Xu, W., and Xu, X. (2022). Sustainable use of CRISPR/Cas in fish aquaculture: the biosafety perspective. Transgenic Res 31, 1–21.
Omori, Y., and Kon, T. (2019). Goldfish: an old and new model system to study vertebrate development, evolution and human disease. J Biochem 165, 209–218.
Ota, K.G., and Abe, G. (2016). Goldfish morphology as a model for evolutionary developmental biology. WIREs Dev Biol 5, 272–295.
Protas, M.E., Hersey, C., Kochanek, D., Zhou, Y., Wilkens, H., Jeffery, W. R., Zon, L.I., Borowsky, R., and Tabin, C.J. (2006). Genetic analysis of cavefish reveals molecular convergence in the evolution of albinism. Nat Genet 38, 107–111.
Radhakrishnan, A., Rohatgi, R., and Siebold, C. (2020). Cholesterol access in cellular membranes controls hedgehog signaling. Nat Chem Biol 16, 1303–1313.
Ramachandra Rao, S., and Fliesler, S.J. (2021). Cholesterol homeostasis in the vertebrate retina: biology and pathobiology. J Lipid Res 62, 100057.
Saito, A., Pietromonaco, S., Loo, A.K.C., and Farquhar, M.G. (1994). Complete cloning and sequencing of rat gp330/"megalin," a distinctive member of the low density lipoprotein receptor gene family.. Proc Natl Acad Sci USA 91, 9725–9729.
Soltis, P.S., and Soltis, D.E. (2016). Ancient WGD events as drivers of key innovations in angiosperms. Curr Opin Plant Biol 30, 159–165.
Storm, T., Heegaard, S., Christensen, E.I., and Nielsen, R. (2014). Megalin-deficiency causes high myopia, retinal pigment epithelium-macromelanosomes and abnormal development of the ciliary body in mice. Cell Tissue Res 358, 99–107.
Sun, Y., and Zhu, Z. (2019). Designing future farmed fishes using genome editing. Sci China Life Sci 62, 420–422.
Suzuki, T., and Tomita, Y. (2008). Recent advances in genetic analyses of oculocutaneous albinism types 2 and 4. J Dermatol Sci 51, 1–9.
Tong, J.F., Zhou, L., Li, S., Lu, L.F., Li, Z.C., Li, Z., Gan, R.H., Mou, C.Y., Zhang, Q.Y., Wang, Z.W., et al. (2021). Two duplicated *ptpn6* homeologs cooperatively and negatively regulate RLR-mediated IFN response in hexaploid gibel carp. Front Immunol 12, 780667.
Van de Peer, Y., Mizrachi, E., and Marchal, K. (2017). The evolutionary significance of polyploidy. Nat Rev Genet 18, 411–424.
Veth, K.N., Willer, J.R., Collery, R.F., Gray, M.P., Willer, G.B., Wagner, D. S., Mullins, M.C., Udvadia, A.J., Smith, R.S., John, S.W.M., et al. (2011). Mutations in zebrafish *lrp2* result in adult-onset ocular pathogenesis that models myopia and other risk factors for glaucoma. PLoS Genet 7, e1001310.
Wang, T., Li, Z., Yu, Z.X., Wang, Z.W., Lian, Z.Q., Du, W.X., Zhao, X., Wang, M.T., Miao, C., Ding, M., et al. (2021). Production of YY males through self-fertilization of an occasional hermaphrodite in Lanzhou catfish (*Silurus lanzhouensis*). Aquaculture 539, 736622.
Wang, M.T., Li, Z., Ding, M., Yao, T.Z., Yang, S., Zhang, X.J., Miao, C., Du, W.X., Shi, Q., Li, S., et al. (2022a). Two duplicated *gsdf* homeologs cooperatively regulate male differentiation by inhibiting *cyp19a1a* transcription in a hexaploid fish. PLoS Genet 18, e1010288.
Wang, Y., Li, X.Y., Xu, W.J., Wang, K., Wu, B., Xu, M., Chen, Y., Miao, L. J., Wang, Z.W., Li, Z., et al. (2022b). Comparative genome anatomy reveals evolutionary insights into a unique amphitriploid fish. Nat Ecol Evol 6, 1354–1366.
Ye, Q.C., and Qu, L.M. (2017). Goldfish of China Descriptions and Illustrations of Diverse Goldfish in China. Fuzhou: The Straits Publishing & Distributing Group.
Yu, P., Wang, Y., Yang, W.T., Li, Z., Zhang, X.J., Zhou, L., and Gui, J.F. (2021). Upregulation of the PPAR signaling pathway and accumulation of lipids are related to the morphological and structural transformation of the dragon-eye goldfish eye. Sci China Life Sci 64, 1031–1049.
Zhao, X., Li, Z., Ding, M., Wang, T., Wang, M.T., Miao, C., Du, W.X., Zhang, X.J., Wang, Y., Wang, Z.W., et al. (2021). Genotypic males play an important role in the creation of genetic diversity in gynogenetic gibel carp. Front Genet 12, 691923.
Zhou, L., and Gui, J. (2017). Natural and artificial polyploids in aquaculture. Aquacul Fisheries 2, 103–111.
Zhou, L., Wang, Z.W., Wang, Y., and Gui, J.F. (2018). Crucian carp and gibel carp culture. In: Gui, J.F., Tang, Q.S., Li, Z.J., Liu, J.S., and De Silva, S.S., ed. Aquaculture in China: Success Stories and Modern Trends. Oxford: John Wiley & Sons. 149–157.

SUPPORTING INFORMATION

The supporting information is available online at https://doi.org/10.1007/s11427-022-2194-7. The supporting materials are published as submitted, without typesetting or editing. The responsibility for scientific accuracy and content remains entirely with the authors.